

UvA-DARE (Digital Academic Repository)

Determining photon flux and effective optical path length in intensified flow photoreactors

Zondag, Stefan D. A.; Schuurmans, Jasper H. A.; Chaudhuri, Arnab; Visser, Robin P. L.; Soares, Cíntia; Padoin, Natan; Kuijpers, Koen P. L.; Dorbec, Matthieu; van der Schaaf, John; Noël, Timothy

DOI

[10.1038/s44286-024-00089-3](https://doi.org/10.1038/s44286-024-00089-3)

Publication date

2024

Document Version

Final published version

Published in

Nature Chemical Engineering

License

Article 25fa Dutch Copyright Act (<https://www.openaccess.nl/en/policies/open-access-in-dutch-copyright-law-taverne-amendment>)

[Link to publication](#)

Citation for published version (APA):

Zondag, S. D. A., Schuurmans, J. H. A., Chaudhuri, A., Visser, R. P. L., Soares, C., Padoin, N., Kuijpers, K. P. L., Dorbec, M., van der Schaaf, J., & Noël, T. (2024). Determining photon flux and effective optical path length in intensified flow photoreactors. *Nature Chemical Engineering*, 1(7), 462–471. <https://doi.org/10.1038/s44286-024-00089-3>

General rights

It is not permitted to download or to forward/distribute the text or part of it without the consent of the author(s) and/or copyright holder(s), other than for strictly personal, individual use, unless the work is under an open content license (like Creative Commons).

Disclaimer/Complaints regulations

If you believe that digital publication of certain material infringes any of your rights or (privacy) interests, please let the Library know, stating your reasons. In case of a legitimate complaint, the Library will make the material inaccessible and/or remove it from the website. Please Ask the Library: <https://uba.uva.nl/en/contact>, or a letter to ~~Library of the University of Amsterdam, Secretariat, Postbox 19185, 1000 BZ Amsterdam, The Netherlands.~~ You will be contacted as soon as possible.

Determining photon flux and effective optical path length in intensified flow photoreactors

Received: 10 December 2023

Accepted: 30 May 2024

Published online: 05 July 2024

 Check for updates

Stefan D. A. Zondag^{1,5}, Jasper H. A. Schuurmans^{1,5}, Arnab Chaudhuri^{2,5}, Robin P. L. Visser², Cíntia Soares³, Natan Padoin³, Koen P. L. Kuijpers⁴, Matthieu Dorbec⁴, John van der Schaaf²✉ & Timothy Noël¹✉

Photocatalysis for small-molecule activation has advanced considerably over the past decade, yet its scale-up remains challenging in part due to photon attenuation effects. One promising solution lies in combining high photonic intensities with continuous-flow reactor technology, requiring careful understanding of photon transport for successful implementation. Here, to address this, we introduce a characterization approach, starting with radiometric light source analysis, followed by three-dimensional reactor and light source simulation. This strategy, when followed up with chemical actinometry experiments, decouples photon flux quantification and path length determination, substantially curtailing the experimental process. The workflow proves versatile across various reactor systems, simplifying intricate light interactions into a single one-dimensional parameter—the effective optical path length. This parameter effectively characterizes photoreactor setups, irrespective of scale, geometry, light intensity or concentration. Additionally, the proposed workflow provides insight into light source positioning and reactor design, and facilitates experiments at lower concentrations, ensuring representative reactor operation. In essence, our approach provides a thorough, efficient and consistent framework for reactor irradiation characterization.

Photons play a pivotal role in modern synthetic chemistry, particularly in the activation of small organic molecules using photocatalysis¹. Their use has the potential to alter the landscape of chemical processes. Of particular interest to the synthesis of pharmaceuticals and agrochemicals is that these reactions often unfold under remarkably benign conditions, such as ambient temperature and visible light^{2–5}. While photocatalysis is well integrated on a smaller scale, such as in medicinal chemistry, its upscaling often presents notable challenges^{6–8}. First, the sheer number of photons required for large-scale photocatalytic transformations necessitates several kilowatts of optical power to produce compounds in substantial quantities. Second, the attenuation of light as it travels through the reactor diminishes its intensity,

leading to undesirable variations in kinetic rates that can, in turn, trigger byproduct formation. Given these complexities, there is an evident demand for precise modeling and straightforward characterization of photochemical reactor technology, providing essential guidance for chemical process engineers.

The successful design of photochemical processes hinges on two key factors: identifying the number of absorbed photons and deciphering its correlation to the production of the desired compound⁹. The former encompasses the irradiation profile within the reactor, where the average path length of photons emerges as a pivotal element. The latter revolves around the quantum yield, a metric that enumerates reactive events per absorbed photon^{10,11}. Traditionally,

A full list of affiliations appears at the end of the paper. ✉ e-mail: j.vanderschaaf@tue.nl; t.noel@uva.nl

chemical actinometry studies have been the predominant strategy to generate this wealth of information¹². Yet, the experimental conditions demanded by actinometric measurements pose challenges^{13,14}. Further complicating matters, the inherent variability in light intensity over a light source's lifespan necessitates laborious recalibrations through actinometry.

In this Article, in our pursuit to further improve the characterization and scalability of photocatalytic processes, we introduce a streamlined workflow that separates the photon flux determination from traditional actinometry experiments and allows for the acquisition of another key parameter, the effective optical path length. To showcase its efficacy, the workflow was validated on a batch setup and subsequently applied to two distinct intensified continuous-flow photoreactors: a capillary reactor and a rotor–stator spinning disk reactor (pRS-SDR). With the burgeoning interest in photocatalysis within industrial contexts, we posit that our approach is paramount for a nuanced comprehension of vital photochemical processes, paving the way for scale-ups from laboratory to pilot and, eventually, commercial levels. Additionally, our strategy offers a deeper dive into the energy balance of photochemical reactions, a crucial component for future operational expense analyses of the entire process¹⁵.

Chemical actinometry for intensified photoreactor platforms

To fully appreciate the need for our proposed workflow, an in-depth understanding of photon behavior in photochemical systems is vital. Chemical actinometry has long served as a cornerstone technique for determining quantum yield and photon flux in photochemical processes. While it has proven invaluable in many traditional settings, its applicability and accuracy come into question when transitioning to photochemical reactor platforms with highly transmitting characteristics¹⁶. These advanced reactor systems, designed for enhanced efficiency and throughput, introduce a set of complexities that can challenge the conventional actinometric methods. Here, we discuss the specific limitations and constraints of employing chemical actinometry in such intensified settings, underscoring the need for advanced approaches to reactor characterization.

The quantum yield plays a pivotal role in the mechanistic exploration of photochemical reactions. It stands as a primary determinant of requisite photon equivalents⁹. This parameter offers insights into the reaction mechanism, such as chain reactions, and benchmarks the efficiency of the photochemical process^{17–20}. As such, ensuring the precision of the quantum yield becomes imperative. This necessitates knowledge of the system's photon flux (expressed in mol s^{-1} , or commonly as E s^{-1} , where einstein represents a mole of photons)²¹. To acquire this, chemical actinometry emerges as the conventional method for obtaining these data. Specifically, chemical actinometry leverages reactions with established quantum yields to experimentally deduce the photon flux²², guided by the Bouguer–Lambert–Beer law (equation (1) and Extended Data Fig. 1a). This law describes the transmittance of light (T) as a change in light intensity (I) against its initial value (I_0), due to the absorbance (A) within a uniform, isotropic medium. The absorbance increases when light traverses a known distance (l) through an attenuating medium that is characterized by the concentration of the absorbing species (C) and its (decadic) molar attenuation coefficient (ϵ).

For any given (photo)chemical system, a molar balance can be derived, as illustrated in equation (2) using an exemplary chemical actinometry batch experiment under ideal conditions, such as perfect mixing^{16,23,24}. In this context, the rate at which the number of moles of species i changes over time (dN_i/dt) is governed by the photon flux reaching the medium ($q_{n,p}$). This is further influenced by the light absorbed by the attenuating species i , represented as the fraction of light that the system does not transmit ($1 - T$), and the known quantum yield of the reaction (ϕ).

$$T = \frac{I}{I_0} = 10^{-A} = 10^{-\epsilon Cl} \quad (1)$$

$$\frac{dN_i}{dt} = -\phi q_{n,p} (1 - T) = -\phi q_{n,p} (1 - 10^{-\epsilon_i C_i l}) \quad (2)$$

In photochemical reactions, not every photon emitted by the light source interacts with the reaction mixture. Factors such as the positioning of the reactor relative to the light source, reflection losses and other material interferences play a role. Those photons that do penetrate the reaction mixture contribute to the initial intensity (I_0), defined at the inner surface of the reactor. This is the interface where the reactor material meets the reaction mixture. Subsequently, the decline in light intensity within the reaction mixture is governed by the concentration of the attenuating species and its molar attenuation coefficient. It is also influenced by the distance the light covers within the medium. This distance, termed the optical path length, serves as an average descriptor of the setup's layout and is independent of the absorbing species properties. This optical path length parameter should not be confused with the commonly used penetration depth, given as the distance light travels before its transmittance has decreased to $e^{-1} \approx 0.37$, which is highly dependent of the absorbing species properties.

It is essential to clarify that the absorbance term for a single-phase system, represented by $A = \epsilon_i C_i l$, can ideally be divided into two distinct components. The first component is influenced by the attenuation properties of the species within the homogeneous medium, denoted by $\epsilon_i C_i$. The second, the path length l , is exclusively affected by the configuration of the reactor and light source. In scenarios with high concentrations, potent absorbing species or extended path lengths, most of the photons are absorbed. This leads to pronounced absorbance values and, consequently, minimal transmittance. As a result, the fraction of light absorbed by the system (represented by the $1 - T$ term in equation (2)) approaches unity, implying the reactor absorbs virtually all incoming light. This scenario streamlines the molar balance, rendering the precise depiction of the optical path length in the system redundant. Hence, variations in this path length would have negligible repercussions on the overall molar balance.

Another prevalent simplification in determining the photon flux hinges on the presumption of a linear rate of change. Typically, this is achieved by conducting experiments over brief irradiation durations, ensuring minimal chemical conversion. With the understanding that a system with low chemical conversions almost entirely absorbs incoming light, equation (2) can be further simplified to deduce the photon flux, as illustrated in equation (3).

$$q_{n,p} \approx -\frac{\Delta N_i}{\Delta t \phi} \quad (3)$$

In recent times, there has been a shift toward conducting photochemical reactions in intensified photoreactors. These reactors combine short path lengths with potent light sources, aiming to amplify productivity and selectivity via uniform irradiation profiles and increased photon intensities^{25,26}. Such intensified systems are at the forefront of sustainable and reliable photochemical scale-ups, attracting considerable interest from both industry and academia^{27,28}. Some prominent reactor examples include microcapillary reactors, vortex type and oscillatory reactors^{29–33}. However, given the attenuation characteristics of a reaction mixture, a crucial aspect to underscore here is that these short-path-length reactors often do not absorb all photons in a single pass. As a result, photons can effectively leave the system, leading to a scenario where complete absorption is not achieved (that is, $T \neq 0$), as illustrated in Extended Data Fig. 1b. To account for these unabsorbed photons, a precise measure of the optical path length becomes essential. This measurement is especially critical when the

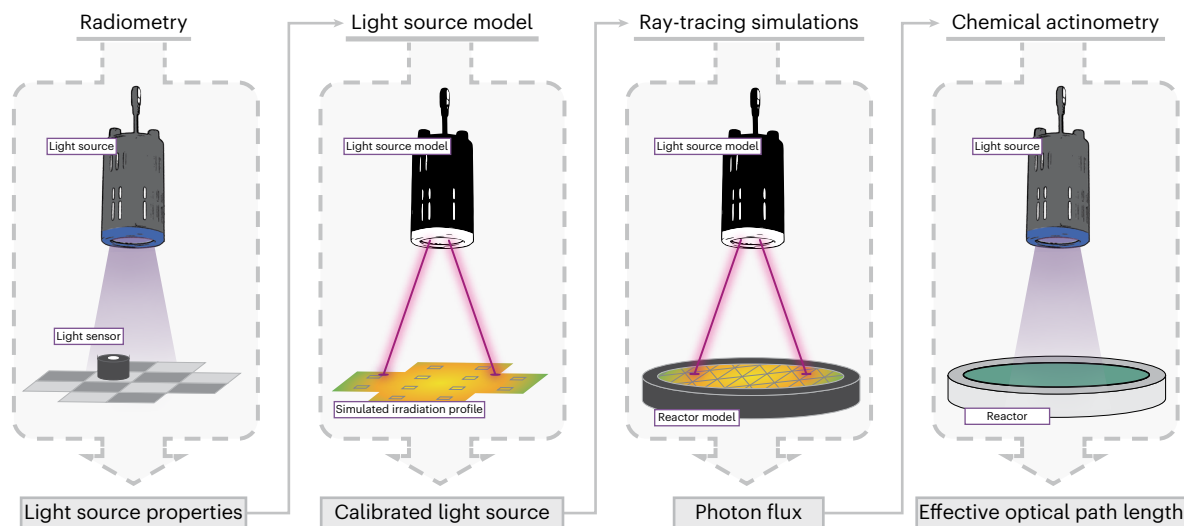


Fig. 1 Schematic representation of the proposed workflow. The four main steps of the workflow for the characterization of photoreactors: radiometry, light-source modeling, ray-tracing simulations and chemical actinometry. These steps are used to obtain the photon flux and effective optical path length.

mixture's attenuation characteristics vary, such as when determining the quantum yield for different photochemical reactions using an identical setup (Supplementary Section 10).

Within the context of full absorption, we define a photon-efficient photoreactor primarily by its relatively long effective optical path length. From an energy efficiency point of view, this enables full use of the received radiant power, and interestingly, as the Bouguer–Lambert–Beer law only portrays relative intensity, this classification remains somewhat detached from the employed optical power. It is worth noting, however, that, with high-power light sources, the system's attenuation properties (like the concentration of absorbing entities) can undergo rapid alterations. High chemical conversions achieved within short irradiation times can transform a photon-efficient setup into a non-photon-efficient one, causing the light transmission to transition from nearly zero to a notable fraction in a short time span (for more details, see Supplementary Section 9).

While strides have been made in discerning the photon flux in intensified reactors, challenges remain. Various methods have been proposed to sustain high absorbance (meaning low actinometer conversion) and prevent product precipitation—these include shortening irradiation times or introducing pulsation^{34,35}. Yet, inaccuracies in path length can still profoundly skew the photon flux measurements in intensified systems. Deriving the path length purely on the basis of geometry, such as using reactor diameter or other geometrical approximations, is not always reliable. This is because light sources come with unique emission distribution patterns, and factors such as refraction, back reflection and total internal reflection can alter the effective optical path length^{14,16,36,37}. While spectro-radiometric measurements offer a way to delineate the system's path length^{38,39}, their precision can be compromised in scenarios with uneven irradiation fields or when bulky light sensors are paired with micro-scaled (or intensified) reactors⁴⁰. Furthermore, achieving accuracy becomes more challenging when interfaces of materials, each having distinct refractive indices, affect the local irradiation profile.

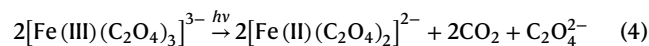
Introduction of the workflow

In light of the challenges presented, we introduce a workflow (Fig. 1) that decouples photon flux quantification and optical path length determination, eliminating the need for laborious and repetitive experimental work. Here, we rely on radiometry to capture data regarding the light intensity of employed light sources. Leveraging these data, a light source model is formulated, which then facilitates the simulation of the

photon flux reaching the reaction mixture. This simulation employs ray tracing^{41–43}, taking into account the reactor's material composition and geometric design. Equipped with this insight, the experimental outcomes of chemical actinometry are repurposed to discern the effective optical path length rather than the photon flux. This alleviates constraints on the absorbance in actinometry experiments, simplifying data collection by enabling exploration of extended irradiation times or diminished concentrations. This versatile approach, adaptable across a range of systems, simplifies intricate light interactions into a singular, one-dimensional parameter: the effective optical path length. This systematic approach not only streamlines reactor characterization but also enhances the accuracy and reproducibility of photochemical processes.

Results

In this study, we utilized the widely recognized potassium ferrioxalate actinometer (equation (4))^{12,18,44,45}, of which the quantum yield has been explored across an extensive wavelength and temperature range⁴⁶. We employed several pseudo-monochromatic ultraviolet (UV)-A light-emitting diode (LED) light sources, and their spectral distributions were determined using a spectrophotometer (Supplementary Fig. 4). The decadic molar attenuation coefficients for the potassium ferrioxalate complex and its subsequent products were measured for relevant wavelengths within the emission spectra (Supplementary Fig. 8). An important conclusion from these measurements is the minimal attenuation coefficient of the resultant products compared with the initial material. This underscores the potassium ferrioxalate complex as the principal absorbing species, simplifying the absorbance assessment.



Validation of the workflow

The presented workflow can be split into two distinguishable parts, namely photon flux quantification and effective optical path length determination. We sought to experimentally validate the first part of the workflow that relies on simulation, namely the photon flux quantification, with a photon-efficient reactor system. Our first experiments, therefore, targeted a basic setup anticipated to have a sufficiently long effective optical path length and mixing (set to 1,100 r.p.m.) to meet the requirements of a photon-efficient system, making the initial behavior path length independent. Hereto, we employed a batch configuration,

which consisted of a test tube (13 mm inner diameter, 15 mm outer diameter) filled with the reaction mixture and illuminated by a high-power LED light source. This off-the-shelf lamp offers four distinct power settings, enabling us to evaluate the same batch setup across four separate data sets. We used a combination of radiometric measurements, three-dimensional (3D) modeling and ray-tracing simulations to assess the photon flux received by the reaction mixture and validated the obtained results with conventional chemical actinometry. Fundamentally, our methodology zeroes in on an exhaustive characterization of the light source, harnessing these data to fine-tune a corresponding model and subsequently applying this model to a virtual rendition of the experimental setup.

We initiated our study with radiometric measurements, utilizing a calibrated light sensor strategically positioned within a pre-established grid. This setup facilitated the precise mapping of light intensity across an irradiated plane. Using the physical dimensions of the light source, we crafted a 3D model and simulated the radiometric conditions using ray tracing within the COMSOL Optics Module (detailed in Methods). This virtual model of the light source was complemented by another model of our experimental batch configuration, with a focus on maintaining authentic system dimensions. Our simulation, leveraging ray tracing, took into account the Fresnel reflection and refraction occurring at the interfaces of media with varying refractive indices. This allowed us to ascertain the intensity incident on the reaction mixture (illustrated in Fig. 2a). By integrating these data over the entirety of the receiving surface, the photon flux ($q_{n,p}$) could be determined for all four power settings of the light source (Fig. 2b).

Next, the chemical actinometry experiments were carried out for the batch system (Fig. 2d and Methods) and the results are shown in Fig. 2b,c, which demonstrate excellent agreement between the simulated and actual photon fluxes. To determine the absorbance of the polychromatic light, we employed a modified version of equation (2), factoring in the lamp's spectral distribution and the wavelength-specific attenuation coefficients. This information facilitated our modeling of the reaction progression over irradiation time, as detailed in Supplementary Sections 2–4, resulting in the kinetic curves displayed in Fig. 2c. In examining the unreacted reaction mixture, the initial spectrum-average transmittance through the reaction tube is estimated at approximately 0.1% when the inner diameter is assumed as the effective optical path length. However, it is crucial to note that not all light will enter the reactor tube through its center; thereby, not all light will perceive the inner diameter as the effective path length. Given that the tube is irradiated from a single side, a popular approach for a cylinder is the employment of a geometric average path length (equation (5))¹⁶. This average can be deduced through integration or, more straightforwardly by visualizing the cylinder as a flat plate, where the total volume is divided by its projected irradiated area (Supplementary Fig. 11):

$$\langle l \rangle = \frac{\text{Cylinder volume}}{\text{Projected area}} = \frac{\pi R^2 H}{2RH} = \frac{\pi R}{2} \approx 1.57R, \quad (5)$$

where $\langle l \rangle$, R and H are the geometric average optical path length, the inner radius and height of the cylinder, respectively. In our analysis, using the geometric average, we calculated an initial spectrum-average transmittance of ~0.3%—a minuscule value. The negligible difference in transmittance between these two path length measures reveals that the average absorbed fraction ($1 - T$, so 0.999 and 0.997, respectively) is practically independent of the path length. This confirms the nature of this setup as a photon-efficient system, wherein almost the entire photon flux is absorbed.

Although the exact measurement of the effective optical path length is not a requirement for larger diameter batch reactor, our methodology (for an overview of the workflow, see Extended Data Fig. 2) underscores the validity of radiometric data collection and

3D modeling to acquire detailed photon flux information. This is evidenced by the strong correlation between the experimental outcomes and the simulated data shown in Fig. 2b. Such congruence virtually eliminates the necessity of conducting chemical actinometry experiments in photon-efficient systems.

Application of the workflow to intensified flow photoreactors

To further illustrate the workflow of photon flux determination through radiometry and ray tracing, we applied the same course of action to two distinct intensified reactor systems. The first system is a well-established microcapillary flow reactor, one of the common laboratory-scale reactor types that have seen wide applicability due to their operational simplicity, low-cost fabrication and ease of assembly^{47,48}. The second is the high-shear spinning disk reactor⁴⁹, specifically the pRS-SDR^{31,50}. Unlike the batch reactor, these intensified reactors function in a continuous-flow mode, presenting the potential for scaling up photochemistry. Importantly, the two selected intensified systems vary considerably in their operation, reactor geometry, light source, scale and reactor-light source configuration, showcasing the versatility of our workflow (for an overview of the workflows, see Extended Data Figs. 3 and 4).

Microcapillary reactor

A custom continuous-flow reactor was assembled using a microcapillary (1.6 mm inner diameter, 3.2 mm outer diameter) coiled around a cylindrical base, which was then placed inside a larger cylindrical chamber. The chamber's inner wall was fitted with an LED strip aligned to irradiate the coiled capillary (Fig. 3d). To characterize the light source, light intensity was measured at specified input powers within the chamber, with the coiled reactor removed during the assessment. The LED strip, with its helical design, was then modeled to calibrate the radiant power essential for the photon flux simulations (Supplementary Section 2). For the simulations, a 3D model of the coiled capillary reactor was created. This model was virtually illuminated through ray tracing, as illustrated in Fig. 3a.

In our study, the LED strip's input current and resultant potential were adjustable, enabling us to test and simulate multiple distinct power settings. The rational lower and upper boundaries of the possible photon fluxes received by the microcapillary reactor are given by the experimental minimum and the radiometric maximum (Fig. 3b). This lower boundary is determined experimentally from the measured initial conversion of the chemical actinometer, assuming all light gets absorbed. The upper boundary is estimated from the integration of the irradiated surface with the radiometric light intensity, emulating the maximum radiant power that can be received. Ray-tracing simulations then revealed photon fluxes of 0.85 and 1.8 $\mu\text{mol s}^{-1}$ received for two distinct power settings (equivalent to 0.27 and 0.56 W optical power). The acquisition of the experimental data (Fig. 3c) was achieved through variation of the flow rate while maintaining a constant reactor volume. We juxtaposed the experimental outcomes with modeled kinetic curves, produced using the molar balance for the capillary reactor under the assumption of it functioning as an ideal plug flow reactor (Supplementary Section 4). In these findings, we differentiate between two path lengths: the effective optical path length, denoted as \bar{l} , and the geometric average path length, $\langle l \rangle$ which is defined in equation (5) for any cylinder irradiated on one side. For the capillary tube, which has an inner diameter of 1.6 mm and an outer diameter of 3.2 mm, the expected geometric average path length is 1.25 mm. This translates to an initial absorbed photon fraction of roughly 0.53, underlining the considerable transmittance. However, the effective optical path lengths determined for this system stood at 1.9 mm and 1.8 mm for the 21 W and 52 W settings, respectively. These determined effective optical path lengths notably exceed the geometric average path length (that is, 1.25 mm), leading to a greater initial absorbed photon fraction

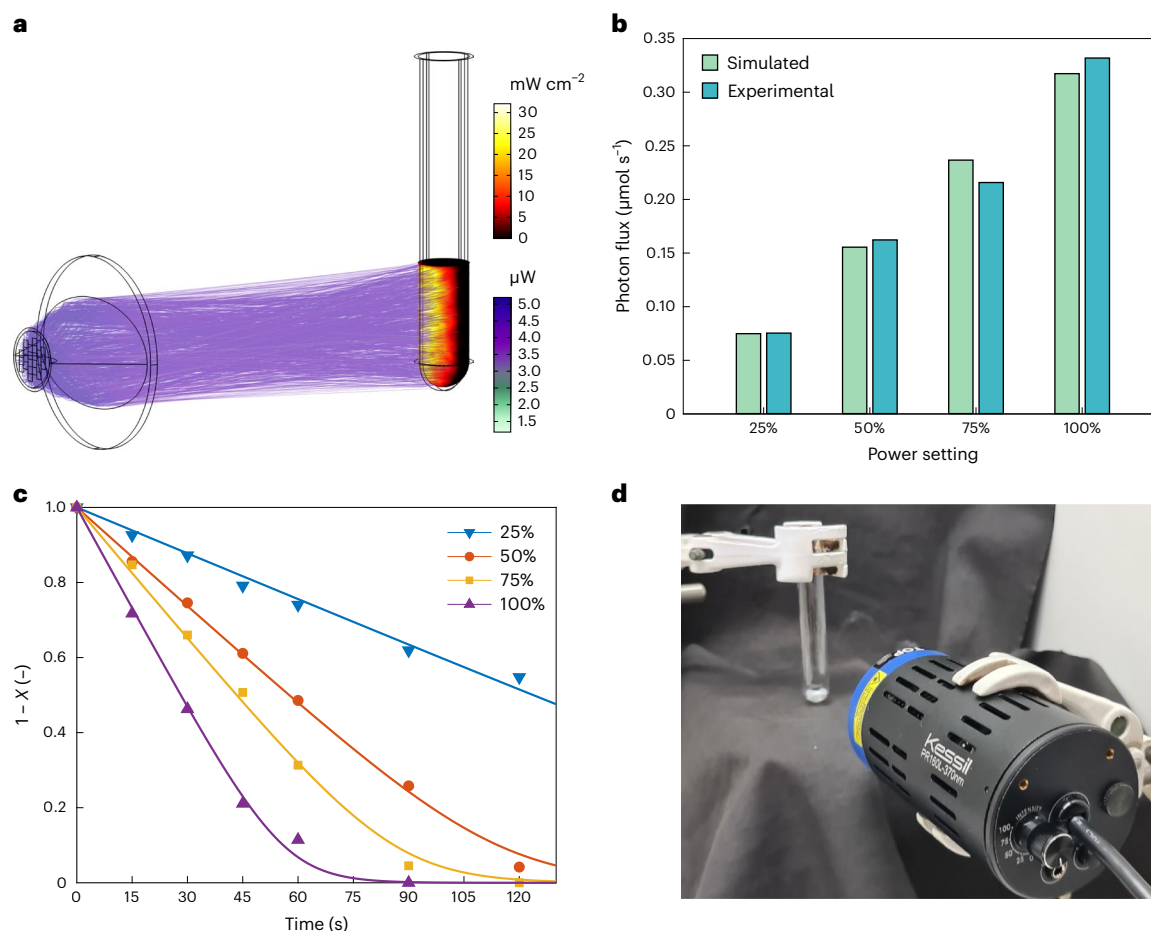


Fig. 2 | Overview of the validation of the workflow results using a batch setup.

a, The irradiation profile (intensity in mW cm^{-2}) and a selection of rays (and their energy in microwatts) reaching the reaction mixture in the batch tube.

b, A comparison of the determined photon flux through ray-tracing simulations and fitting using experimental data for the four tested power settings. **c**, The experimental data and kinetic curves for the investigated batch system, showing the nonconverted fraction $1 - X$ of the potassium ferrioxalate actinometer.

d, The experimental batch setup, with the lamp positioned 10 cm from the tube. The simulation in **a** was performed for the 100% power setting (43 W input electrical power), using 24 LEDs with 3×10^4 photons each, 2.4×10^4 of those interacting with the reaction mixture, with only a selection of 1×10^3 of those shown for visualization. For the effective optical path length for the photon flux determination in **b** and **c** the geometric average (l) = 10.3 mm from equation (5) was used.

of approximately 0.66 and, consequently, a higher conversion rate. As can be seen in Fig. 3c, employing the conventional geometric average path length resulted in less precise alignment with the experimental data. Utilizing the geometric average path length to correlate photon fluxes with experimental data, as commonly practiced in traditional chemical actinometry, yielded considerably elevated flux values. However, due to the inherent limitations imposed by rational boundaries, these flux values appear unrealistic when compared with the radiometric maxima (Fig. 3b).

Several factors might contribute to the unexpected increase in path length. First, the LED strip's inherent noncollimated nature—given its beam angle of around 60° —allows light to enter at varied angles, thereby extending the path length within the medium. Additionally, the tube's curvature and coiling alter the angle at which light hits the air–capillary interface, impacting both reflection and, more crucially, refraction. Given the transparent polymer material of the capillary possesses a refractive index higher than the surrounding air, light is refracted inward toward the reaction mixture, generally lengthening the path.

The inward refraction of incoming light causes more than just the elongation of the effective optical path length. It also modifies the photon flux received by the reaction mixture. This effect stems from an expanded surface area available for collecting irradiation

(see Supplementary Section 8 for details). To illustrate, when the light source's intensity was measured with radiometry, the sensor registered approximately 2.8 mW cm^{-2} (for 21 W input electrical power). However, when the simulated photon flux is assessed over the inner capillary's projected area (as shown in equation (5), $2RH$), the value rises to 4.5 mW cm^{-2} . This phenomenon arises because the light interacting with the capillary's outer surface refracts inward, concentrating the light on the exposed reaction mixture. As a result, the light is collected by the flat projected outer surface of the capillary, not the inner one. In other words, the light received by the outer area is focused on a smaller reaction medium area, resulting in the concentrated value of 4.5 mW cm^{-2} .

Subsequent experiments with doubled and quadrupled actinometer concentrations were conducted to underscore the importance of accurate path length determination in low-transmittance systems (Supplementary Fig. 9). With elevated concentrations, the absorption characteristics (ϵC) of the reaction mixture became predominant, shifting the initial reactor conditions toward photon-efficient behavior characterized by almost complete absorption of the light.

In another set of experiments, we explored the potential impact of the cylindrical capillary holder's surface. While previous experiments utilized a nonreflective black surface for this cylinder, optimizing energy utilization could involve making this surface reflective to

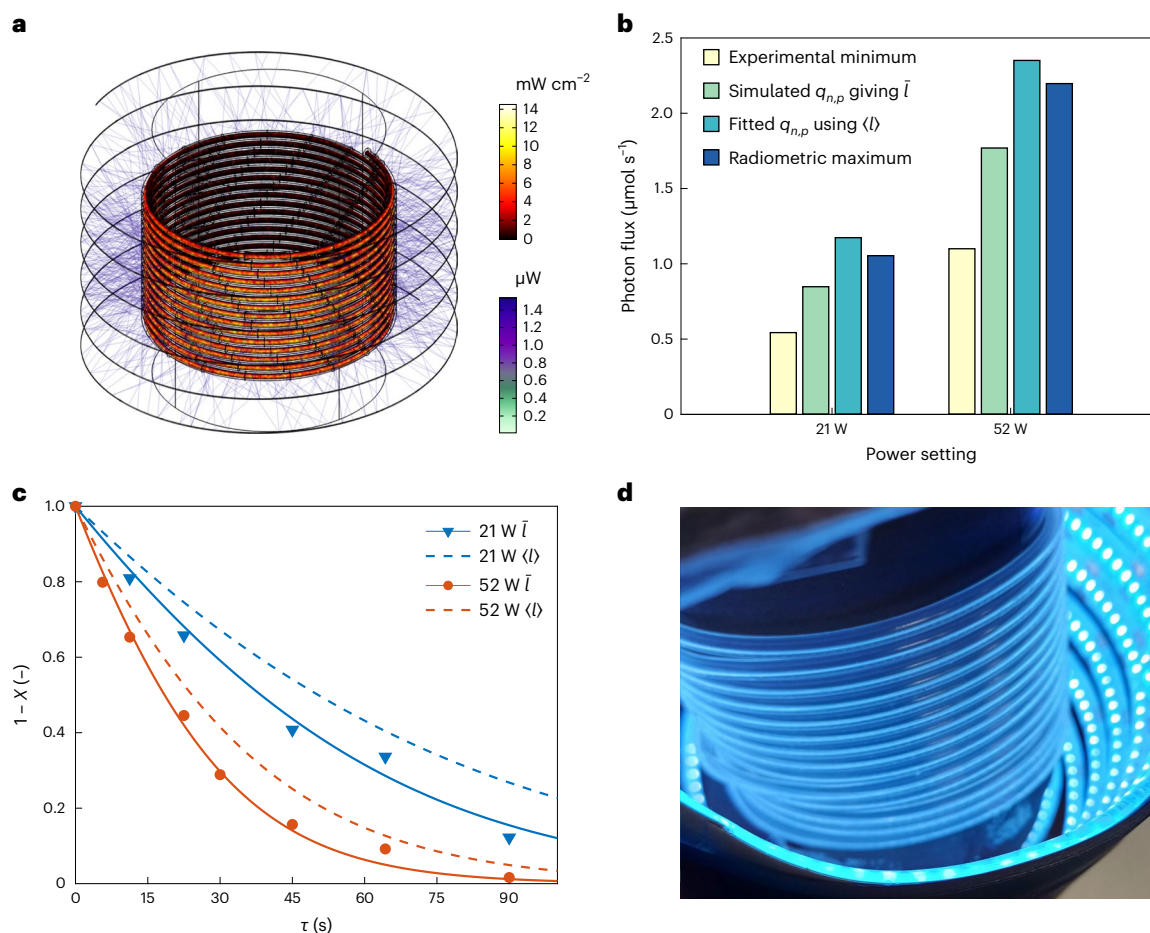


Fig. 3 | Overview of the results for the microcapillary reactor. **a**, The irradiation profile (intensity in mW cm^{-2}) and a selection of rays (and their energy in microwatts) reaching the reaction mixture in the coiled capillary reactor. **b**, A comparison of the determined photon fluxes for the two tested power settings. **c**, The experimental data and kinetic curves for the investigated capillary reactor system, showing the nonconverted fraction $1 - X$ of the potassium ferrioxalate actinometer as a function of residence time τ , for the

effective optical path length $\bar{l} = 1.85$ mm and the geometric average path length $\langle l \rangle = 1.25$ mm. **d**, The experimental microcapillary reactor setup, opened and lifted for the picture. The simulation in **a** was performed for the 52 W power setting (that is, input electrical power), using 576 LEDs with 2×10^3 photons each, 4.8×10^5 of those interacting with the reaction mixture, with only a selection of 2×10^3 of those shown for visualization.

increase photon absorption. This enhancement would manifest in two primary ways: first, by amplifying the received flux and, second, by extending the effective path length of the previously received irradiation. The enhanced flux would arise from initially missed irradiation being reflected back toward the capillary, offering another opportunity for interaction with the absorbing medium. In contrast, the extended path length would come from transmitted irradiation—already passed through the reaction mixture—being reflected for another pass. Simulations with a reflective supporting cylinder, assuming lossless specular reflection, indeed showed an increase in total received photon fluxes for both power settings, reaching 1.0 and $2.2 \mu\text{mol s}^{-1}$ (equivalent to 0.33 and 0.69 W optical power received by the reaction mixture), representing a 22% boost of the photon flux due to the reflective material. When combining these fluxes with experimental data, the effective optical path length extended to ~ 2.3 mm (Supplementary Fig. 9).

pRS-SDR

The subsequent reactor analyzed was the intensified continuous pRS-SDR. This setup incorporated the reactor and an LED-based floodlight, both housed within stainless-steel casing (Fig. 4d)^{31,50}. The reactor's design features a fast rotating disk (the rotor) encased in narrow-fitting housing, called the stator. The irradiation process is facilitated through a quartz window, serving as the upper stator.

Comprehensive characterization of the floodlight was undertaken, which was then integrated into a detailed model of the entire assembly, as depicted in Fig. 4a.

The floodlight was designed to function at a singular power setting. Therefore, both the experiments and simulations adhered to this specific power input, resulting in a simulated photon flux received of $12.5 \mu\text{mol s}^{-1}$ (~ 4.1 W optical power received by the reaction mixture). Figure 4c showcases the experimental data obtained under continuous-flow conditions by varying the flow rate at different rotation speeds, along with their corresponding fits. Unlike the microcapillary reactor, the molar balance for the pRS-SDR was developed under the presumption that the reactor emulates the behavior of a continuously stirred tank reactor. This presumption is grounded in previous studies that indicate that continuously stirred tank reactor behavior prevails under standard pRS-SDR operation (Supplementary Section 4)^{51,52}. From the experimental data, it is evident that the rotation speed has a minimal impact on the reaction rate. This suggests that the system operates not in a mass-transfer limited domain but predominantly within a photon-limited regime. The projected geometric average path length for this reactor was estimated at the axial gap distance (that is, the spacing between the quartz stator and rotor), which is 2.0 mm. Based on this value, an initial absorbed photon fraction of ~ 0.78 can be derived.

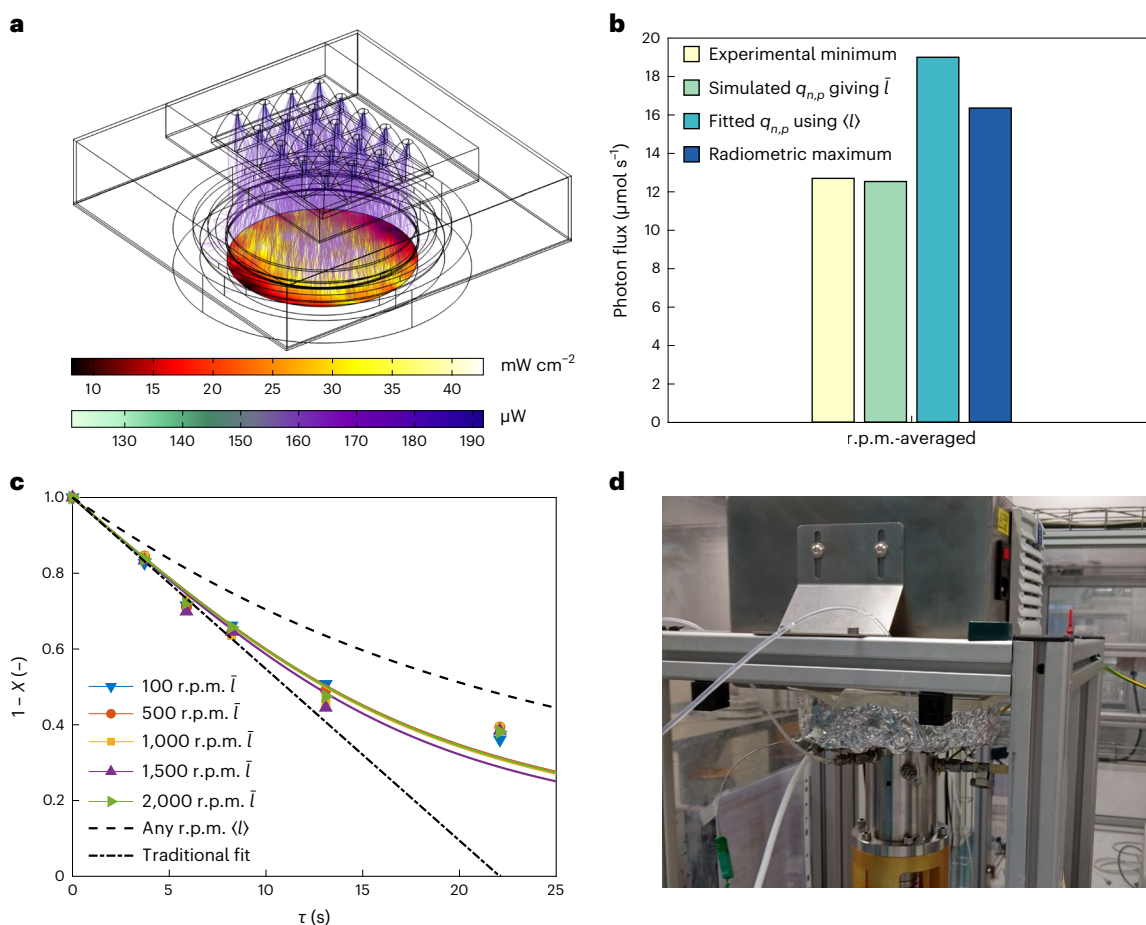


Fig. 4 | Overview of the results for the pRS-SDR. a, The irradiation profile (intensity in mW cm^{-2}) and a selection of rays (and their energy in microwatts) reaching the reaction mixture in the pRS-SDR. **b**, A comparison of the determined photon fluxes for the pRS-SDR. r.p.m., revolutions per minute. **c**, The experimental data and kinetic curves for the investigated pRS-SDR system, showing the nonconverted fraction $1 - X$ of the potassium ferrioxalate

actinometer as a function of residence time τ , for their effective optical path lengths (average of $\bar{l} = 5.3$ mm) and the geometric average path length $\langle l \rangle = 2.0$ mm. **d**, The experimental pRS-SDR setup. The simulation in **a** was performed for a power input of 175 W, using 20 LEDs with 1.5×10^3 photons each, 2.4×10^4 of those interacting with the reaction mixture, with only a selection of 1×10^3 of those shown for visualization.

The effective optical path length, however, was found to be 5.3 ± 0.2 mm, notably larger than the geometric average path length of 2.0 mm. Employing this effective optical path length, an initial absorbed photon fraction of ~0.98 can be derived, intrinsically resulting from the close agreement between the experimentally determined minimum and simulated photon flux (Fig. 4b). Absorption of the majority of photons gives a markedly enhanced conversion rate and, in comparison with the microcapillary reactor (Fig. 4b), a lower fraction of photons transmitted.

Intriguingly, substantial chemical conversions—typically observed at prolonged residence times—are essential to discern the notable impact of path length variations. This phenomenon is evident in the initial gradient of the kinetic curves depicted in Fig. 4c. At such low conversions, the disparity between different path lengths seems minimal. However, as conversion increases, the curves noticeably diverge, with the effective optical path length playing an increasingly dominant role in the kinetics and the accuracy of the models. Using conventional photon flux determination methods, which assume complete absorption of the incident light, and fitting a linear model to the initial gradient (the traditional fit in Fig. 4c), an average received photon flux of $12.7 \mu\text{mol s}^{-1}$ (~4.1 W optical power received by the reaction mixture) is found. This contrasts only marginally with the flux determined via radiometry and ray tracing, which was less than 2% lower. Interestingly, if one were to apply the known gap distance of 2.0 mm, the fitted received photon

flux approximates $19.0 \mu\text{mol s}^{-1}$ (~6.2 W optical power received by the reaction mixture). This value not only exceeds the radiometric maximum but also the total radiant power of the floodlight (~5.3 W emitted by the light source) as determined with radiometry and ray tracing, rendering this as an implausible outcome (all discussed fluxes are shown in Fig. 4b).

Several factors could account for the evident discrepancy between the anticipated and fitted path lengths. The light source's beam angle affects the angle of incidence and, in turn, the initial single-pass path length. Additionally, the stainless-steel rotor might reflect light back into the system, allowing for a second pass. Another factor to consider is the phenomenon of total internal reflection, stemming from the pronounced refractive index difference at the quartz–air interface, which can confine a portion of the photons within the system. Given the knowledge that the initial transmittance following the determined 5.3 mm effective optical path length is virtually negligible, categorizing this reactor as a photon-efficient system becomes unexpectedly justified (Supplementary Section 9). This highlights that the importance of accurate path length determination is intimately tied to the dimensions, and the absorbing attributes of the medium.

Discussion

In this study, we present a comprehensive workflow to separately ascertain the photon flux and effective optical path length for intensified

photoreactors. Recognizing that the effective optical path length in photochemical reactors and setups is challenging to define with a single predetermined value, we proposed its determination through a synergistic approach involving radiometry, ray tracing and chemical actinometry. We conducted radiometric measurements to quantify light intensity across multiple distinct points, factoring in potential light source degradation. This information serves as a calibration benchmark for virtual light source simulations. Ray tracing emerges as an invaluable instrument, granting profound insights into light sources and photoreactors^{42,53,54}. Our approach, though necessitating precise light source and reactor representations, proves capable at handling even reactors with complex geometries and nontrivial effective optical path lengths. Only a description of the reactor's outer surface and reactor–medium interface suffices for determining the received photon flux, thereby obviating complex photon path assessments within ray-tracing software.

The outcome of our ray-tracing simulations and experimental endeavors aims to shed light on irradiation profiles and photon absorption, offering predictive capabilities for absorption properties across diverse photochemical systems. Additionally, by integrating the unique geometry of different reactor designs, photon fluxes and effective path lengths can be ascertained through data fitting from a single kinetic experimental curve. Our methodology underwent validation using a batch reactor, allowing its application to be extended to determining both photon flux and effective optical path length in a microflow reactor and a pRS-SDR. Intriguingly, the effective optical path length derived did not mirror the results obtained by using the frequently applied geometric average path length, underscoring the pivotal roles played by factors such as diffuse emission, reflection and refraction. Indeed, using the geometric average path length when deducing photon flux was found to defy physical possibility, given the constraints of the light sources and radiometric data at hand. This revelation underscores the paramount importance of accurately obtaining effective optical path lengths and attests to the robustness of our proposed workflow.

While our method has been exemplified through the widely used ferrioxalate actinometer in intensified reactors, its applicability spans other chemical actinometers across varied configurations. Essential prerequisites include the quantum yield of the reaction, the attenuation properties of the actinometer and formed products and the light source emission characteristics. Moreover, meticulous detailing of the geometries of the light source, light sensor and photoreactor interfaces facilitates a representative portrayal within streamlined ray-tracing simulations.

This workflow offers invaluable insights into photochemical reactor systems, serving as an essential tool for process engineers in the industry. Not only does it hold the potential to enhance energy balance evaluations, but it also stands as a pivotal asset for conducting operational expenditure assessments by facilitating foresight in anticipating and optimizing material usage. Furthermore, the workflow leads to efficient scale-up studies by enabling straightforward characterization and design of systems.

Methods

Chemical actinometry

Potassium ferrioxalate has been used as chemical actinometer, and the experimental procedure was based on literature^{12,55}. The potassium ferrioxalate was either directly used from the supplier (Alfa Aesar) or made by mixing iron(III)chloride (Sigma-Aldrich) with di-potassium oxalate (Sigma-Aldrich) in a 1:3 mole ratio. The product was obtained by crystallization, which was performed two times, whereafter the crystals were placed in a desiccator to dry.

A solution of 6 mM of potassium ferrioxalate in 50 mM sulfuric acid (Sigma-Aldrich) solution, using demineralized water as solvent, was prepared. The solution was loaded in the batch reactor or pumped

through the microcapillary/pRS-SDR, under the irradiation of a UV light source (batch reactor: Kessil PR160L 370 nm (first generation), input power 43 W; microcapillary reactor: LuxaLight UV-A 365 nm LED strip, input power 52 W; pRS-SDR: UV-A curing 365 nm floodlight, input power 175 W). The reactor was placed at a known position relative to the light source. The batch test tube (Pyrex, inner diameter 13.2 mm, outer diameter 15.2 mm, filled with 4 ml reaction mixture) was stirred, using a magnetic stirrer and stirrer bar (1,100 r.p.m.). This tube was removed after the set irradiation time, whereafter a sample was taken. A new unirradiated tube was used to obtain the subsequent data point to ensure that the volume inside the reactor remained constant. For the continuous reactor types, samples were taken at the outlet after waiting several residence times to ensure steady-state conditions. The microcapillary reactor (perfluoro alkoxy alkane, 1.6 mm inner diameter, 3.2 mm outer diameter, 7.5 ml) was operated in continuous mode rather than using stop-flow, due to increased mixing and prevention of unwanted dilution^{13,24}. For the pRS-SDR, the flow rate in combination with the total volume was used to express the residence time (59 ml excluding connections, ~28 ml irradiated volume). All experiments and the preparation of the solutions and samples were conducted in a darkroom.

The samples (0.1 ml) were diluted with water (1.4 ml), and after dilution 0.6 ml was added to a buffer solution (2.0 ml). The buffer consisted of 6 mM 1,10-phenanthroline (Sigma-Aldrich), 0.6 M sodium acetate (Sigma-Aldrich) in 0.18 M sulfuric acid, using demineralized water as solvent. The samples were measured using a UV-visible spectrophotometer (UV-2501PC, Shimadzu) in a 1 cm quartz cuvette at the absorption peak of the formed complex found at 510 nm.

Radiometry

Radiometric characterization of the light sources was performed with a UV light sensor (RM12 Sensor Opsytec Dr. Göbel UVA+) that could be placed at a known position relative to the light source, in a predefined grid. After fixation of the sensor, proper shielding of the environment was ensured, whereafter the light source was turned on. The light intensity after stabilization of the value was noted. A dark experiment was conducted to account for any possible background irradiation.

Ray tracing

For the development of the light source and reactor setup simulations, geometric representations of the light sources and reactors were made on the basis of the measured dimensions. These representations, including material properties, were modeled in COMSOL Multiphysics 5.4. For the radiometric ray-tracing calibration, the UV sensor used for the experimental data was recreated as well. The simulations were conducted using the Geometric Optics module with the time-dependent solver, with time stepping calculated with the generalized alpha algorithm. Moreover, the solution of the linear system of equations proceeded iteratively with the GMRES method. Here, the relevant release information (direction vector, emission profile, ray properties and total power) could be defined. The irradiated surface (either the sensor or reaction mixture) was defined as an accumulator that freezes the incident ray and deposits the ray's power onto the surface. This allowed us to obtain the optical output power of the light source, through calibration of the virtual received intensities to the experimental quantities, as well as estimate the emission profile at the same time (for example, Lambertian, conical or hemispherical emission), by minimizing the error in intensity distribution differences. Both mesh dependency and result convergence studies as a result of simulation size have been performed (Supplementary Section 7).

Nonlinear fitting of effective optical path length

The kinetic curves' molar balances (Supplementary Section 4) were implemented in MATLAB R2022b. A nonlinear least squares method was used to fit the effective optical path length (or photon flux for

the batch system) in the balance. The differential equations were solved with a variable-step, variable-order solver for stiff differential equations.

Data availability

The authors declare that all data obtained and used in this work are available within the article and its Supplementary Information. Source data are provided with this paper.

References

- Marzo, L., Pagire, S. K., Reiser, O. & König, B. Visible-light photocatalysis: does it make a difference in organic synthesis? *Angew. Chem. Int. Ed.* **57**, 10034–10072 (2018).
- Ravelli, D., Dondi, D., Fagnoni, M. & Albini, A. Photocatalysis. A multi-faceted concept for green chemistry. *Chem. Soc. Rev.* **38**, 1999–2011 (2009).
- Liu, J., Lu, L., Wood, D. & Lin, S. New redox strategies in organic synthesis by means of electrochemistry and photochemistry. *ACS Cent. Sci.* **6**, 1317–1340 (2020).
- Crisenza, G. E. M. & Melchiorre, P. Chemistry glows green with photoredox catalysis. *Nat. Commun.* **11**, 803 (2020).
- Candish, L. et al. Photocatalysis in the life science industry. *Chem. Rev.* **122**, 2907–2980 (2022).
- Donnelly, K. & Baumann, M. Scalability of photochemical reactions in continuous flow mode. *J. Flow Chem.* **11**, 223–241 (2021).
- Buglioni, L., Raymenants, F., Slattery, A., Zondag, S. D. A. & Noël, T. Technological innovations in photochemistry for organic synthesis: flow chemistry, high-throughput experimentation, scale-up, and photoelectrochemistry. *Chem. Rev.* **122**, 2752–2906 (2022).
- Zondag, S. D. A., Mazzarella, D. & Noël, T. Scale-up of photochemical reactions: transitioning from lab scale to industrial production. *Annu. Rev. Chem. Biomol. Eng.* **14**, 283–300 (2023).
- Corcoran, E. B., McMullen, J. P., Lévesque, F., Wismer, M. K. & Naber, J. R. Photon equivalents as a parameter for scaling photoredox reactions in flow: translation of photocatalytic C–N cross-coupling from lab scale to multikilogram scale. *Angew. Chem. Int. Ed.* **59**, 11964–11968 (2020).
- Su, Y., Straathof, N. J. W., Hessel, V. & Noël, T. Photochemical transformations accelerated in continuous-flow reactors: basic concepts and applications. *Chemistry* **20**, 10562–10589 (2014).
- Wong, K.-L., Bünzli, J.-C. G. & Tanner, P. A. Quantum yield and brightness. *J. Lumin.* **224**, 117256 (2020).
- Hatchard, C. G. & Parker, C. A. A new sensitive chemical actinometer—II. Potassium ferrioxalate as a standard chemical actinometer. *Proc. R. Soc. Lond. Ser. A* **235**, 518–536 (1956).
- Wriedt, B. & Ziegenbalg, D. Common pitfalls in chemical actinometry. *J. Flow Chem.* **10**, 295–306 (2020).
- Radjagobalou, R. et al. A revised 1D equivalent model for the determination of incident photon flux density in a continuous-flow LED-driven spiral-shaped microreactor using the actinometry method with Reinecke's salt. *J. Flow Chem.* **11**, 357–367 (2021).
- Noël, T. *Photochemical Processes in Continuous-Flow Reactors* (World Scientific, 2017).
- Roibu, A. et al. An accessible visible-light actinometer for the determination of photon flux and optical pathlength in flow photo microreactors. *Sci. Rep.* **8**, 5421 (2018).
- Megerle, U., Lechner, R., König, B. & Riedle, E. Laboratory apparatus for the accurate, facile and rapid determination of visible light photoreaction quantum yields. *Photochem. Photobiol. Sci.* **9**, 1400–1406 (2010).
- Cismesia, M. A. & Yoon, T. P. Characterizing chain processes in visible light photoredox catalysis. *Chem. Sci.* **6**, 5426–5434 (2015).
- Scaiano, J. C. A beginners guide to understanding the mechanisms of photochemical reactions: things you should know if light is one of your reagents. *Chem. Soc. Rev.* **52**, 6330–6343 (2023).
- Swierk, J. R. The cost of quantum yield. *Org. Process Res. Dev.* **27**, 1411–1419 (2023).
- Braslavsky, S. E. et al. Glossary of terms used in photocatalysis and radiation catalysis (IUPAC recommendations 2011). *Pure Appl. Chem.* **83**, 931–1014 (2011).
- Noël, T. & Zysman-Colman, E. The promise and pitfalls of photocatalysis for organic synthesis. *Chem Catal.* **2**, 468–476 (2022).
- Maafi, M. & Brown, R. G. The kinetic model for AB(1 ϕ) systems. *J. Photochem. Photobiol. A* **187**, 319–324 (2007).
- Wriedt, B. & Ziegenbalg, D. Application limits of the ferrioxalate actinometer. *ChemPhotoChem* **5**, 947–956 (2021).
- Sambigioglio, C. & Noël, T. Flow photochemistry: shine some light on those tubes! *Trends Chem.* **2**, 92–106 (2020).
- Williams, J. D. & Kappe, C. O. Recent advances toward sustainable flow photochemistry. *Curr. Opin. Green Sustain. Chem.* **25**, 100351 (2020).
- Loubière, K., Oelgemöller, M., Aillet, T., Dechy-Cabaret, O. & Prat, L. Continuous-flow photochemistry: a need for chemical engineering. *Chem. Eng. Process. Process Intensif.* **104**, 120–132 (2016).
- De Risi, C. et al. Recent advances in continuous-flow organocatalysis for process intensification. *React. Chem. Eng.* **5**, 1017–1052 (2020).
- Russo, D. et al. Direct photolysis of benzoyllecgonine under UV irradiation at 254nm in a continuous flow microcapillary array photoreactor. *Chem. Eng. J.* **283**, 243–250 (2016).
- Lee, D. S. et al. Scalable continuous vortex reactor for gram to kilo scale for UV and visible photochemistry. *Org. Process Res. Dev.* **24**, 201–206 (2020).
- Chaudhuri, A. et al. Process intensification of a photochemical oxidation reaction using a rotor–stator spinning disk reactor: a strategy for scale up. *Chem. Eng. J.* **400**, 125875 (2020).
- Wen, Z. et al. Optimization of a decatungstate-catalyzed C(sp³)-H alkylation using a continuous oscillatory millistructured photoreactor. *Org. Process Res. Dev.* **24**, 2356–2361 (2020).
- Wan, T. et al. Accelerated and scalable C(sp³)-H amination via decatungstate photocatalysis using a flow photoreactor equipped with high-intensity LEDs. *ACS Cent. Sci.* **8**, 51–56 (2022).
- Wriedt, B., Kowalczyk, D. & Ziegenbalg, D. Experimental determination of photon fluxes in multilayer capillary photoreactors. *ChemPhotoChem* **2**, 913–921 (2018).
- Vandekerckhove, B., Piens, N., Metten, B., Stevens, C. V. & Heugebaert, T. S. A. Practical ferrioxalate actinometry for the determination of photon fluxes in production-oriented photoflow reactors. *Org. Process Res. Dev.* **26**, 2392–2402 (2022).
- Sender, M., Wriedt, B. & Ziegenbalg, D. Radiometric measurement techniques for in-depth characterization of photoreactors—part 1: 2 dimensional radiometry. *React. Chem. Eng.* **6**, 1601–1613 (2021).
- Roibu, A., Mc Carogher, K., Morthala, R. B., Eyckens, R. & Kuhn, S. Modelling approaches to predict light absorption in gas-liquid flow photosensitized oxidations. *Chem. Eng. J.* **452**, 139272 (2023).
- Cornet, J.-F. et al. A simple and reliable method to determine mean incident light flux densities on cylindrical photoreactors and photobioreactors from a unique fluence rate measurement. *Ind. Eng. Chem. Res.* **62**, 4875–4884 (2023).
- Yaghmaei, M. & Scaiano, J. C. A simple Norrish type II actinometer for flow photoreactions. *Photochem. Photobiol. Sci.* **1**, 1865–1874 (2015).

40. Aillet, T., Loubiere, K., Dechy-Cabaret, O. & Prat, L. Accurate measurement of the photon flux received inside two continuous flow microphotoreactors by actinometry. *Int. J. Chem. React. Eng.* **12**, 257–269 (2014).
41. Cambié, D., Zhao, F., Hessel, V., Debije, M. G. & Noël, T. Every photon counts: understanding and optimizing photon paths in luminescent solar concentrator-based photomicroreactors (LSC-PMs). *React. Chem. Eng.* **2**, 561–566 (2017).
42. Kant, P. et al. Isophotonic reactor for the precise determination of quantum yields in gas, liquid, and multi-phase photoreactions. *Chem. Eng. J.* **452**, 139204 (2023).
43. de Oliveira, G. X., Kuhn, S., Riella, H. G., Soares, C. & Padoin, N. Combining computational fluid dynamics, photon fate simulation and machine learning to optimize continuous-flow photocatalytic systems. *React. Chem. Eng.* **8**, 2119–2133 (2023).
44. Shin, N. Y., Ryss, J. M., Zhang, X., Miller, S. J. & Knowles, R. R. Light-driven deracemization enabled by excited-state electron transfer. *Science*. **366**, 364–369 (2019).
45. Hu, H. et al. Metal–organic frameworks embedded in a liposome facilitate overall photocatalytic water splitting. *Nat. Chem.* **13**, 358–366 (2021).
46. Rabani, J., Mamane, H., Pousty, D. & Bolton, J. R. Practical chemical actinometry—a review. *Photochem. Photobiol.* **97**, 873–902 (2021).
47. Plutschack, M. B., Pieber, B., Gilmore, K. & Seeberger, P. H. The Hitchhiker's guide to flow chemistry. *Chem. Rev.* **117**, 11796–11893 (2017).
48. Neyt, N. C. & Riley, D. L. Application of reactor engineering concepts in continuous flow chemistry: a review. *React. Chem. Eng.* **6**, 1295–1326 (2021).
49. Chaudhuri, A. et al. Kinetics and intensification of tertiary amine N-oxidation: towards a solventless, continuous and sustainable process. *Chem. Eng. J.* **416**, 128962 (2021).
50. Chaudhuri, A., Zondag, S. D. A., Schuurmans, J. H. A., van der Schaaf, J. & Noël, T. Scale-up of a heterogeneous photocatalytic degradation using a photochemical rotor–stator spinning disk reactor. *Org. Process Res. Dev.* **26**, 1279–1288 (2022).
51. de Beer, M. M. M., Keurentjes, J. T. F. T. F., Schouten, J. C. C. & van der Schaaf, J. Engineering model for single-phase flow in a multi-stage rotor–stator spinning disc reactor. *Chem. Eng. J.* **242**, 53–61 (2014).
52. de Beer, M. M., Pezzi Martins Loane, L., Keurentjes, J. T. F., Schouten, J. C. & van der Schaaf, J. Single phase fluid–stator heat transfer in a rotor–stator spinning disc reactor. *Chem. Eng. Sci.* **119**, 88–98 (2014).
53. Rochatte, V. et al. Radiative transfer approach using Monte Carlo method for actinometry in complex geometry and its application to Reinecke salt photodissociation within innovative pilot-scale photo(bio)reactors. *Chem. Eng. J.* **308**, 940–953 (2017).
54. Kowalczyk, D., Knorr, G., Peneva, K. & Ziegenbalg, D. Making photocatalysts screenable—a milliscale multi-batch screening photoreactor as extension for the modular photoreactor. *React. Chem. Eng.* **8**, 2967–2983 (2023).
55. Kuhn, H. J., Braslavsky, S. E. & Schmidt, R. Chemical actinometry (IUPAC Technical Report). *Pure Appl. Chem.* **76**, 2105–2146 (2004).

Acknowledgements

We express our gratitude to the molecular photonics group (Van 't Hoff Institute for Molecular Sciences, University of Amsterdam) for using the darkroom and to M. G. Debije (Eindhoven University of Technology) for his assistance with the radiometric measurements. S.D.A.Z., J.H.A.S. and T.N. thank the European Union's Horizon research and innovation program FlowPhotoChem (S.D.A.Z. and T.N.), grant number 862453 and CATART (J.H.A.S. and T.N.), grant agreement number 101046836. A.C. thanks Janssen Pharmaceutica NV for research funding. C.S. and N.P. thank the Coordination for the Improvement of Higher Education Personnel (CAPES, Brazil, grant number 88887.310560/2018-00) and the National Council for Scientific and Technological Development (CNPq, Brazil, grant numbers 313202/2021-4 and 312247/2022-2) for funding. The materials presented and views expressed here are the responsibility of the author(s) only. The EU Commission takes no responsibility for any use made of the information set out.

Author contributions

S.D.A.Z., J.H.A.S. and A.C. designed the project. S.D.A.Z., J.H.A.S., A.C. and R.P.L.V. performed and analyzed the experiments. S.D.A.Z. performed the ray-tracing simulations, with supervision and input from C.S. and N.P. Additionally, C.S., N.P., K.P.L.K. and M.D. provided input and participated in discussions throughout the course of the project. J.v.d.S. and T.N. directed the project. S.D.A.Z., J.H.A.S. and T.N. wrote the paper with input and feedback from all authors.

Competing interests

The authors declare no competing interests.

Additional information

Extended data is available for this paper at <https://doi.org/10.1038/s44286-024-00089-3>.

Supplementary information The online version contains supplementary material available at <https://doi.org/10.1038/s44286-024-00089-3>.

Correspondence and requests for materials should be addressed to John van der Schaaf or Timothy Noël.

Peer review information *Nature Chemical Engineering* thanks the anonymous reviewers for their contribution to the peer review of this work.

Reprints and permissions information is available at www.nature.com/reprints.

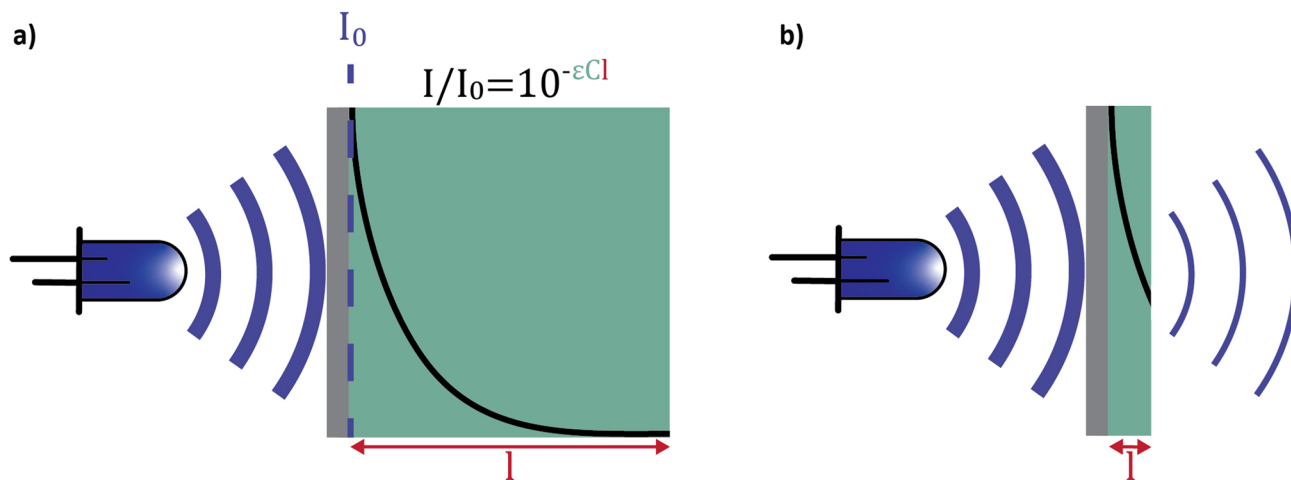
Publisher's note Springer Nature remains neutral with regard to jurisdictional claims in published maps and institutional affiliations.

Springer Nature or its licensor (e.g. a society or other partner) holds exclusive rights to this article under a publishing agreement with the author(s) or other rightsholder(s); author self-archiving of the accepted manuscript version of this article is solely governed by the terms of such publishing agreement and applicable law.

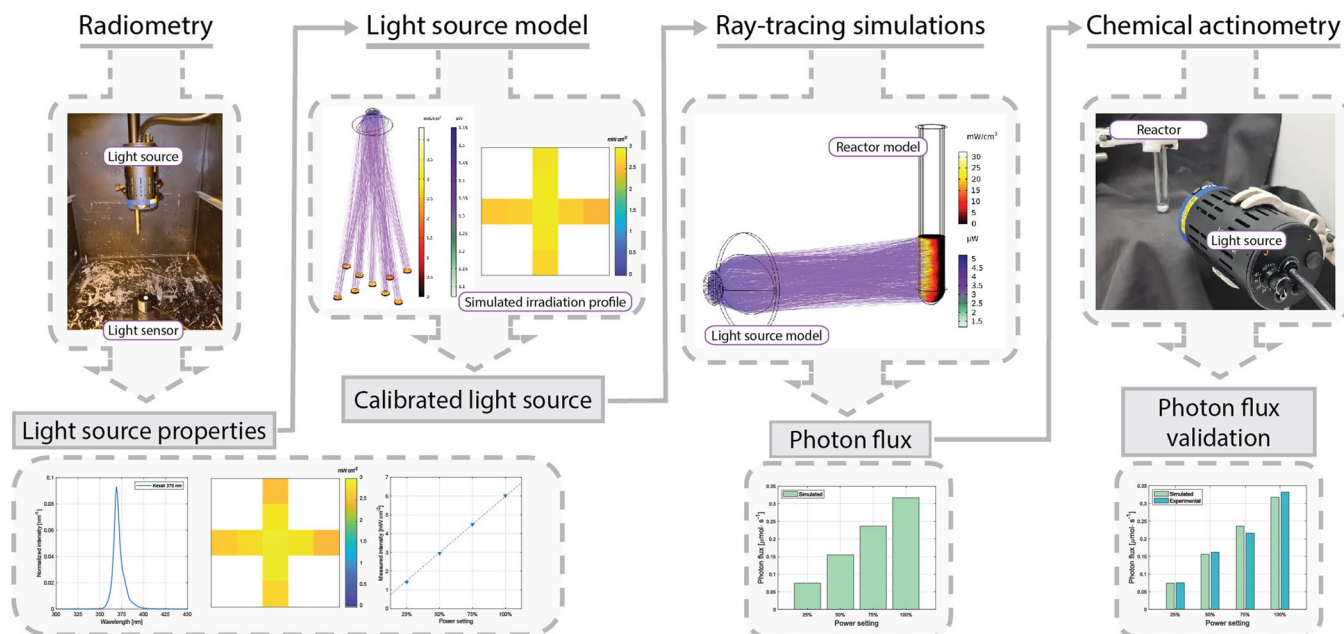
© The Author(s), under exclusive licence to Springer Nature America, Inc. 2024

¹Flow Chemistry Group, Van 't Hoff Institute for Molecular Sciences, Universiteit van Amsterdam, Amsterdam, The Netherlands. ²Department of Chemical Engineering and Chemistry, Sustainable Process Engineering, Eindhoven University of Technology, Eindhoven, The Netherlands. ³Department of Chemical and Food Engineering, Federal University of Santa Catarina, Florianópolis, Brazil. ⁴Technology and Engineering Group, Janssen Research and Development, Beerse, Belgium. ⁵These authors contributed equally: Stefan D. A. Zondag, Jasper H. A. Schuurmans, Arnab Chaudhuri.

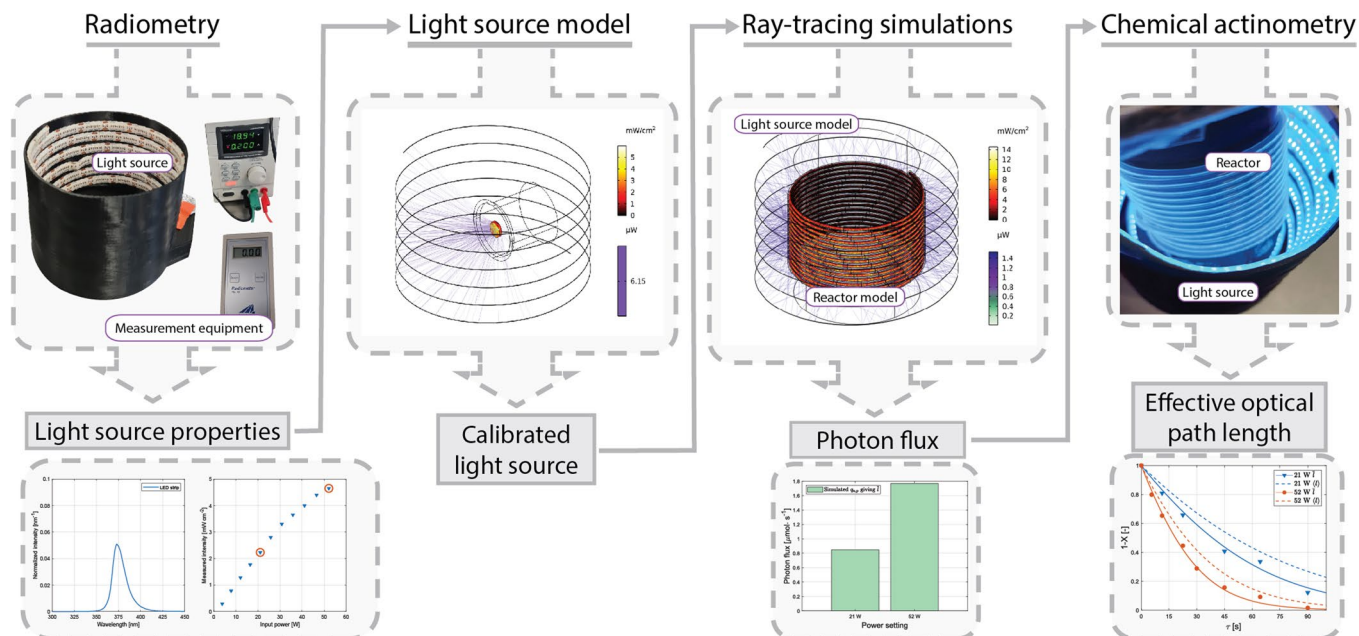
✉ e-mail: j.vanderschaaf@tue.nl; t.noel@uva.nl



Extended Data Fig. 1 | Visualization of the light intensity according to the Bouguer-Lambert-Beer law. a) Visualization of a photon-efficient system with negligible transmittance. **b)** Visualization of a non-photon-efficient system with substantial transmittance.

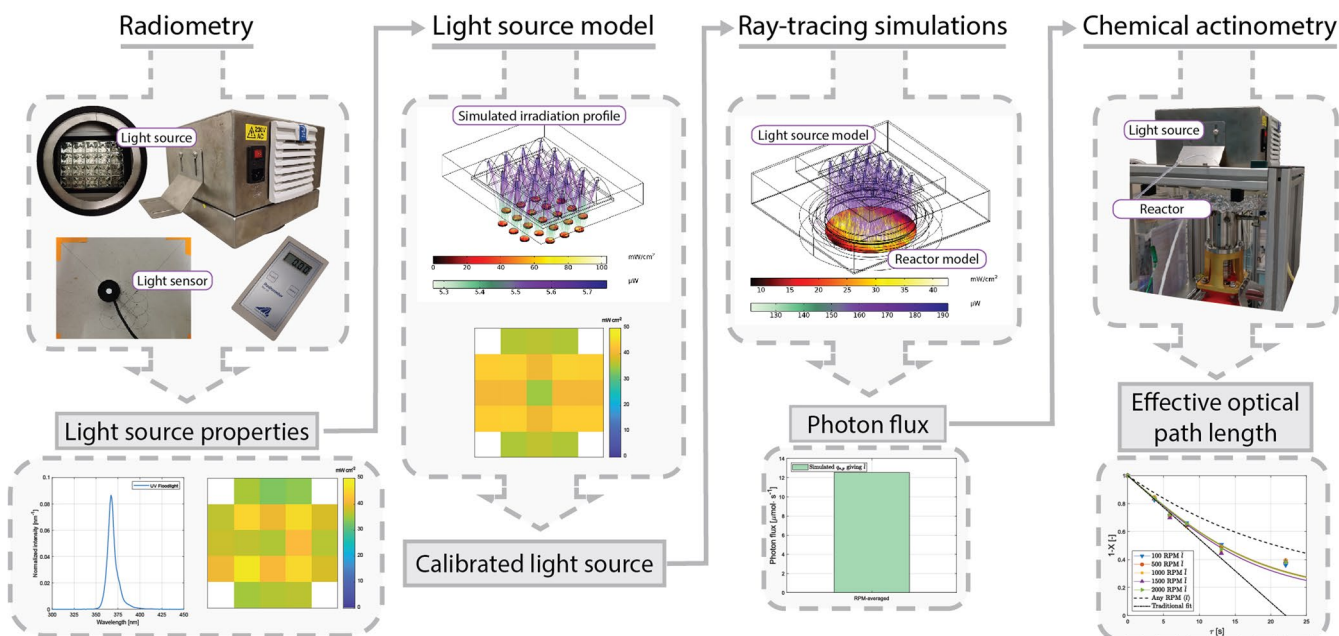


Extended Data Fig. 2 | Detailed visualization of the workflow for the batch configuration. An overview of how the workflow is used to validate the simulated photon flux for the photon-efficient batch configuration. Details on the light source properties and light source model can be found in Section 2 of the Supplementary Information.



Extended Data Fig. 3 | Detailed visualization of the workflow for the microcapillary configuration. An overview of how the workflow is used to determine the effective optical path length through photon flux simulation

and chemical actinometry for the microcapillary configuration. Details on the light source properties and light source model can be found in Section 2 of the Supplementary Information.



Extended Data Fig. 4 | Detailed visualization of the workflow for the pRS-SDR configuration. An overview of how the workflow is used to determine the effective optical path length through photon flux simulation

and chemical actinometry for the pRS-SDR configuration. Details on the light source properties and light source model can be found in Section 2 of the Supplementary Information.